Volumetric Modeling and Experimental Validation of Normal Contact Dynamic Forces

Michael Boos[1]
Ph.D. Student
e-mail: mboos@uwaterloo.ca

John McPhee
Professor
Fellow ASME

Department of Systems Design Engineering,
University of Waterloo,
Waterloo, ON, N2L 3G1, Canada
e-mail: mcphee@uwaterloo.ca

A volumetric contact dynamics model has been proposed for the purpose of generating reliable and rapid simulations of contact dynamics. Forces and moments between bodies in contact can be expressed in terms of the volume of interference between the undeformed geometries. This allows for the modeling of contact between complex geometries and relatively large contact surfaces, while being computationally less expensive than finite element methods. However, the volumetric model requires experimental validation. Models for simple geometries in contact have been developed for stationary and dynamic contact, and an apparatus has been developed to experimentally validate these models. This paper focuses on validation of the normal contact models. Measurements of forces and displacements will be used to identify the parameters related to the normal force, i.e., the volumetric stiffness and hysteretic damping factor for metallic surfaces. The experimental measurements are compared with simulated results to assess the validity of the volumetric model. [DOI: 10.1115/1.4006836]

1 Introduction

The Mobile Servicing System (MSS), Canada's main contribution to the International Space Station (ISS), consists of two manipulators, the Space Station Remote Manipulator System (SSRMS) and the Special Purpose Dextrous Manipulator (SPDM). The MSS is used for assembly and maintenance of the ISS [1]. Tele-operated space-based robotic operations require careful task planning, verification, and training on the ground. The complexity and risk of these operations means that accurate real-time contact dynamics models are required for on-earth simulation and astronaut training.

Many point contact models are unsuitable for situations involving complex or conforming contacts. More complex models, such as finite element models, are far too computationally intensive for real-time simulation. The Canadian Space Agency has applied hardware-in-the-loop simulations (HLS) to determine contact dynamics; however, HLS can be expensive [2].

A volumetric contact model has been proposed for use in generating reliable simulations of space-based manipulator operations. This model has been shown to be applicable to complex and conforming geometries and accounts for angular dynamics ignored by many point contact models such as rolling resistance and spinning friction torque. However, experimental validation of this model is required.

This paper presents a series of experiments used to validate a volumetric normal force model for hard metal-on-metal contact. Common point-contact models and a volumetric contact dynamics model are presented for comparison in Sec. 1. Section 2 describes the quasi-static and dynamic experiments designed to validate the volumetric model, along with the apparatus used to conduct them. Results of these experiments are discussed in Sec. 3, followed by conclusions in Sec. 4.

1.1 Point Contact Models.

Contact is often modeled using *point-contact* models—that is, the region of contact is assumed to be very small relative to the geometries of the bodies, such that contact may be assumed to be occurring at a single point. Gilardi and Sharf [3] describe three common continuous (or compliant) point contact dynamics models: spring-dashpot, the perfectly elastic Hertz model [4], and the damped model of Hunt and Crossley [5].

A common model used in relatively stiff contact for robot modeling is the Kelvin-Voigt model, in which the contacting materials are represented by a spring and dashpot in parallel [6]. The contact model proposed by Hunt and Crossley is a normal force model similar to spring-damper models, where the spring force is based on Hertz theory for linear elastic solids, and the damping is adjusted to avoid the limitations incurred by other models. The Hertz model for contact force is the best known model for contact between two spheres of isotropic material [7]. In order to use this model, a number of assumptions must be made [8]. First, it must be assumed that the contact patch is small relative to the geometries of the bodies. This allows contact to be considered from a single point, where the depth of penetration δ can be measured. Consequently, the surfaces must be nonconforming (i.e., not concave relative to each other where they come into contact). Otherwise, contact might occur at more than one location or be spread out over a wide area. Finally, it is assumed that the bodies are homogenous isotropic, linearly elastic solids.

According to Hertz theory, the contact normal force is given by

$$f_n = k\delta^n \tag{1}$$

The generalized stiffness k is dependent on the shapes and material properties of the surfaces in contact. For two spheres in contact, $n = 3/2$.

The Hertz theory formulation is applicable for spheres in contact under static conditions. However, if pure Hertz theory were to be applied for dynamic contact situations (ignoring friction), no energy would be dissipated in the process of contact. Thus, some damping is necessary [7].

Hunt and Crossley [5] proposed the following model for the contact normal force:

[1]Corresponding author.

Contributed by the Design Engineering Division of ASME for publication in the Journal of Computational and Nonlinear Dynamics. Manuscript received September 19, 2011; final manuscript received April 23, 2012; published online July 23, 2012. Assoc. Editor: Dan Negrut.

$$f_n = K(\delta) + B(\dot{\delta}, \delta) \tag{2a}$$

$$= k\delta^n + (\lambda\delta^n)\dot{\delta} \tag{2b}$$

which is consistent with Hertzian theory for contacting spheres under static conditions for $n = 3/2$.

For low impact velocities and most linear elastic materials [9], the coefficient of restitution e can be approximated for a limited range of values by

$$e = 1 - \alpha\dot{\delta}^{\mathrm{i}} \tag{3}$$

where α is an empirically determined value, and $\dot{\delta}^{\mathrm{i}}$ is the initial impact speed. For hard contact materials, it can then be shown [10] that

$$f_n \approx k\delta^n\left(1 + \frac{3}{2}\alpha\dot{\delta}\right) \tag{4}$$

More recently, by considering the energy stored and dissipated during contact, Flores et al. [11] showed that

$$f_n = k\delta^n\left[1 + \frac{8(1-e)}{5e}\frac{\dot{\delta}}{\dot{\delta}^{\mathrm{i}}}\right] \tag{5}$$

Unlike Eq. (4), Eq. (5) is applicable to both hard and soft materials.

The previous models are fast and efficient. Little effort is required to compute the penetration depth and rate for simple geometries, as well as the contact forces. In addition, the model is continuous in velocities and accelerations, which aids numerical integration and should not introduce discontinuous disturbances for control. The static contact force in the models is based on physical theory, yielding high fidelity for low-speed impact as long as assumptions about the size and shape of the contact region hold. Experimentally, the model has been shown to be more accurate than the Kelvin-Voigt spring-damper model [12]. The normal contact force can be combined with Coulomb or other models to determine sliding friction forces [3].

For certain geometries, stiffness k can be determined from material properties [8]. Gilardi and Sharf [3] note that the determination of contact parameters such as damping or coefficient of restitution is highly dependent on the particular configuration and geometry of contact. For some contact scenarios, parameters are determined through tuning to match simulation and experimental results, as with Stoianovici and Hurmuzlu [13].

The efficiency of point contact models make them useful for modeling granular flows using the discrete element method, which involve contact between many bodies. Vu-Quoc et al. developed an elastoplastic normal force-displacement model by correcting a Hertzian model to account for plastic deformation [14,15]. This normal force model was successfully validated using drop tests and compression tests on soybeans [16] and for columns of polystyrene particles [17].

However, not all contact scenarios involve relatively small contact patches or simple, nonconforming geometries. In these cases, other models are required to accurately simulate contact. In addition, point contact models ignore the rotational effects of contact. A complete contact model would need to account for torques derived from rolling resistance and spinning friction.

1.2 Volumetric Model. A flexible volumetric contact dynamics model has been proposed by Gonthier et al. [18]. This model allows for more complex and conforming geometries where point contact models may be inadequate because contact surfaces are relatively large or where closed-form solutions from elastic theory are not available. It can be shown that the model also accounts for angular dynamics such as rolling resistance and spinning friction torque.

For larger or conforming contact surfaces, a Winkler elastic foundation model [8] has been used. The Winkler model assumes a pressure distribution from one surface deforming as a "bed of springs" to comply with the contacting surface. This model has been adapted to contact dynamics. The forces and moments between two bodies in contact can be expressed directly in terms of the volume of interference V between the undeformed geometries of the bodies.

This paper considers only the case for the volumetric model where one of the two bodies is assumed to be flexible, while the other is rigid, as depicted in Fig. 1. Gonthier [19] also demonstrates a contact model where both bodies are assumed deformable, for which the equations governing contact forces are identical to the one-body case.

Volumetric Properties. In the one deformable body contact model depicted in Fig. 1, one of the bodies $\mathcal{B}_{\mathrm{i}}$ is flexible, while the other $\mathcal{B}_{\mathrm{j}}$ is perfectly rigid. The contact surface S is assumed to be a flat surface on $\mathcal{B}_{\mathrm{j}}$.

The volume of interference, that is, the volume $\mathcal{B}_{\mathrm{i}}$ is compressed by, is given by

$$V = \int_S \delta(\mathbf{s})dS = \int_V dV \tag{6}$$

where S is the contact surface, and $\delta(\mathbf{s})$ is the depth of penetration at point s on the contact surface, as depicted in Fig. 1. The vector $\mathbf{n}$ is defined as unit vector normal to S.

The centroid of this volume is

$$\mathbf{p}_{\mathrm{c}} = \frac{1}{V}\int_V \mathbf{p}dV \tag{7}$$

where $\mathbf{p}$ is the position vector to a point in the volume.

The weighed surface centroid $\mathbf{s}_{\mathrm{c}}$ is given by

$$\mathbf{s}_{\mathrm{c}} = \frac{1}{V}\int_S \mathbf{s}\delta(\mathbf{s})dS \tag{8}$$

Gonthier et al. demonstrate that the volumetric and surface centroids are collinear along the unit vector $\mathbf{n}$ [18].

Another relevant property is the contact surface second moment of area $\mathbf{J}_{\mathrm{s}}$ weighted by penetration depth,

$$\mathbf{J}_{\mathrm{s}} = \int_S ((\boldsymbol{\rho}_{\mathrm{s}} \cdot \boldsymbol{\rho}_{\mathrm{s}})\mathbf{I} - \boldsymbol{\rho}_{\mathrm{s}}\boldsymbol{\rho}_{\mathrm{s}})\delta(\mathbf{s})dS \tag{9}$$

where $\boldsymbol{\rho}_s$ is a vector from the centroid $\mathbf{p}_c$ to the point s on the surface. This can be approximated by the volume inertia tensor

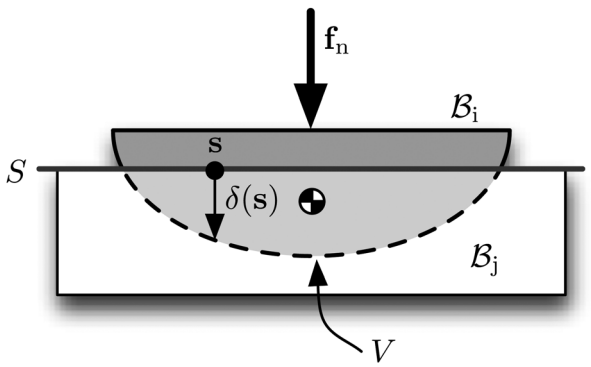

Fig. 1 Volume of interference between two bodies in contact

$$\mathbf{J}_s \approx \mathbf{J}_v = \int_V ((\boldsymbol{\rho}_v \cdot \boldsymbol{\rho}_v)\mathbf{I} - \boldsymbol{\rho}_v \boldsymbol{\rho}_v) dV \tag{10}$$

where $\boldsymbol{\rho}_V$ is a vector from the centroid $\mathbf{p}_c$ to the point $\mathbf{p}$ in the volume.

Normal Force. In this model, the contact normal force is related directly to the size of the volume of interference through a volumetric stiffness k_v, given in units of force per unit volume. The normal force is given by [18]

$$\mathbf{f}_n = k_v V(1 + a v_{cn})\mathbf{n} \tag{11}$$

where a is a velocity-dependent hysteretic damping parameter and v_{cn} is the speed of the centroid in the normal direction $\mathbf{n}$. (Speed v_{cn} is analogous to speed $\dot{\delta}$ used in point contact models.) This force acts normal to the contact surface, through the centroid of the volume.

Note that Eq. (11) is very similar in form to Eq. (4) for the point-based Hunt-Crossley model. Hysteretic behavior is dependent on the speed of contact. For free collision, the parameter a can be shown to depend on only the coefficient of restitution e and the initial impact velocity v_{cn}^i [2],

$$a = \frac{d}{e v_{cn}^i} \tag{12}$$

where d is related to e by

$$\frac{1 + d/e}{1 - d} = e^{d(1+1/e)} \tag{13}$$

which can be approximated as

$$d \approx 1 - e^2 \tag{14}$$

Roy and Carretero build on this volumetric normal force model [20] by having the damping depend on the rate of change for the volume dV/dt rather than the product of the normal speed of the contact centroid Vv_{cn}. However, this may cause discontinuities in normal forces at impact if the geometries are conforming. In Gonthier's model, forces should always be continuous.

Rolling Resistance Torque. As motion in the normal direction is damped through the normal contact force, there will also be resistance to tangential rolling, as this rolling causes parts of the contact surface to move in the normal direction. Gonthier et al. [18] found that by integrating the contact pressure distribution over the contact surface, the rolling resistance torque is

$$\tau_r = k_v a \mathbf{J}_s \cdot \omega_t \tag{15}$$

where ω_t is the component of the relative angular velocity between the bodies tangent to the contact surface.

2 Experiments

The purpose of the experiments is to determine parameters for the volumetric contact model and validate that model. Parameters to be determined include a volumetric stiffness constant, a hysteretic damping factor, and friction parameters. Of interest for validation are the volume-normal force relationship, bristle-friction model, spinning friction torque model, and the Contensou effect [18]. The experiments have been divided into those pertaining to the normal contact forces and those for the friction forces. In this paper, only the normal force experiments are described.

For the contact normal force model, measurements of the displacement and forces in the normal direction are required. Two experiments are used to determine and validate both the volumetric stiffness and damping parameters separately.

Two different contact payloads were designed. The first is spherical on a flat plane, and the results from volumetric contact simulation can be compared directly with those from Hertz theory (where the plane is taken as a sphere of infinite radius). The second is cylindrical, with a flat end forming one of the contact surfaces with the opposing plane. This payload does not satisfy the assumptions in Hertz theory of a small contact patch and nonconforming geometries, which allows testing of the volumetric model in cases where Hertz theory does not apply.

In contrast to the complex geometries of space manipulator payloads, the geometric pairs used in these experiments were relatively simple. These primitive geometries facilitated straightforward control, measurement, and modeling of experiments, while providing a contact scenario that could be compared directly to classical point-based models. The choice of a flat cylindrical payload provided a more distributed contact surface, which could not be modeled with point-based models as easily, as would be the case for many space manipulator contact scenarios.

2.1 Volumetric Stiffness. Starting from rest, with the payload touching the contact surface and no forces between them, the force driving the payload is gradually increased so that the force sensors are loaded quasi-statically. The rate in displacement was limited to 12 μm/s, pausing for one second at each programmed position, such that the effect of damping was negligible. Without the effects of damping for the quasi-static case of the volumetric model, the magnitude of force in Eq. (11) becomes

$$F_{QS} = k_v V \tag{16}$$

The measured displacement was used to find the volume of interference so that a volumetric stiffness constant k_v could be estimated through a linear fit of force to volume measurements. In order to estimate the value of the stiffness parameter, the following cost function must be minimized for k_v:

$$c_{vol} = \sum_k \left(F_{meas}^k - k_v V(\delta^k)\right)^2 \tag{17}$$

where F_{meas}^k are the sampled force measurements and $V(\delta^k)$ are estimates of the volume of interference derived from position measurements δ^k and dependent on the payload volume chosen. However, the exact point of contact ($\delta = 0$) is also unknown since the experiment will begin with the payload and contact surface separated. Thus, the point of contact p_0 must also be estimated from the raw position measurements p^k,

$$\delta^k = p^k - p_0 \tag{18}$$

giving a nonlinear optimization problem for minimizing c_{vol} in two parameters, k_v and p_0,

$$c_{vol} = \sum_k \left(F_{meas}^k - k_v V(p^k - p_0)\right)^2 \tag{19}$$

For spherical payloads, results can also be compared with Hertz theory. From Eq. (1) and $n = 3/2$, a different cost function can be determined,

$$c_{Hertz} = \sum_k \left(F_{meas}^k - k(\delta^k)^{3/2})\right)^2 \tag{20a}$$

$$= \sum_k \left(F_{meas}^k - k(p^k - p_0)^{3/2})\right)^2 \tag{20b}$$

giving a least-squares minimization problem for k and p_0.

2.2 Damping. Equation (12) shows that the hysteretic damping factor a in free collision depends on the initial normal velocity

at impact v_{cn}^{i} and a coefficient of restitution e. With a known volumetric stiffness and measured displacements, velocities, and forces, the damping factor and coefficient of restitution can be estimated.

Many experiments for determining the coefficient of restitution in free collision rely on drop testing. For the purposes of our experiments, very low contact velocities of no more than a few millimeters per second, as might be expected in complex robotic space operations, are desired. In order for collisions to be limited to such velocities, drop heights of less than a micron above the contact surface would be required. It would be extremely difficult to accurately position and measure such an experiment with any reasonable precision.

In the case of these experiments, the payload is connected to an actuator to regulate the speed of collision. Thus, the experiments do not involve free collision, and the notion of a coefficient of restitution, either kinetic or kinematic, does not apply.

The payload is brought into contact with the force plate at different motor-driven velocities, and the subsequent forces and displacements are measured. For each case, the damping factor a is estimated. A relationship between a and v_{cn}^{i} will be established, but this relationship cannot be compared back with a coefficient of restitution as with Gonthier [19].

To estimate the hysteretic damping parameter from measured results, the forces measured during quasi-static experiments can be compared with those measured when the payload is in motion. The force under damping should be given by

$$F_{\text{damped}} = F_{\text{QS}}(1 + av_{\text{cn}}) \tag{21}$$

where F_{QS} is the estimated force with no damping from Eq. (16). To estimate the value of the damping parameter, the following cost function must be minimized:

$$c_{\text{damp}} = \sum_{k} \left(F_{\text{meas}}^{k} - F_{\text{QS}}^{k}(1 + av_{\text{cn}}^{k}) \right)^2 \tag{22}$$

where F_{meas}^{k} are the sampled force measurements, and F_{QS}^{k} are the quasi-static force estimates from the position data, calculated using Eq. (16). The speeds v_{cn}^{k} are estimated using a first-order central finite difference approximation of the position data,

$$v_{\text{cn}}^{k} = \frac{d\delta^{k}}{dt} \approx \frac{\delta^{k+1} - \delta^{k-1}}{t^{k+1} - t^{k-1}} \tag{23}$$

2.3 Apparatus. An apparatus has been developed to experimentally validate the proposed volumetric models, as shown in Fig. 2. The apparatus has two configurations, one for validating the normal contact models and the other for the friction models. The normal configuration uses a ball-screw linear actuator to drive a rigidly mounted payload into a normal contact surface, which is mounted to a force transducer with a configured resolution of 0.1 N. Payload position relative to the contact surface is measured through a linear encoder, with a resolution of up to 1.22 nm.

The normal configuration with a cylindrical payload is depicted in Fig. 3. A 316 stainless steel payload is rigidly clamped to the linear actuator. Also rigidly attached to the actuator is a linear encoder, which measures the position of the payload relative to a glass reference grating. This reference is rigidly mounted to the force sensor.

Contact Surfaces. Different deformable contact surfaces can be mounted in front of the piezoelectric force sensor. Metal contact surfaces were employed, an aluminum plate and a thicker AZ31 magnesium alloy. The aluminum (6061) plate was 25.4 mm thick and polished to 1200 grit. The AZ31 magnesium alloy was 22 mm thick and loaded perpendicular to the extruded direction. The

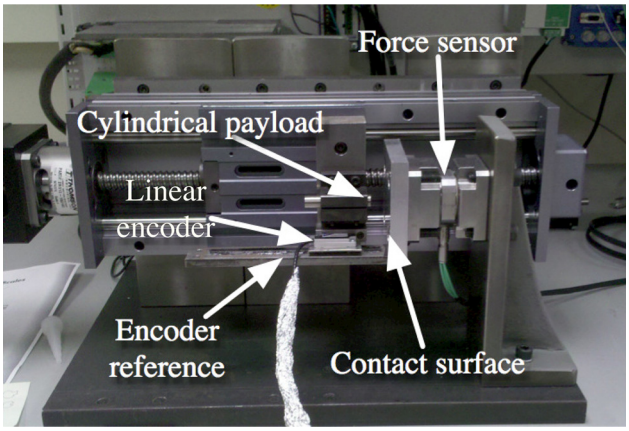

Fig. 2 Mechanical apparatus for contact experiments, shown in the normal configuration

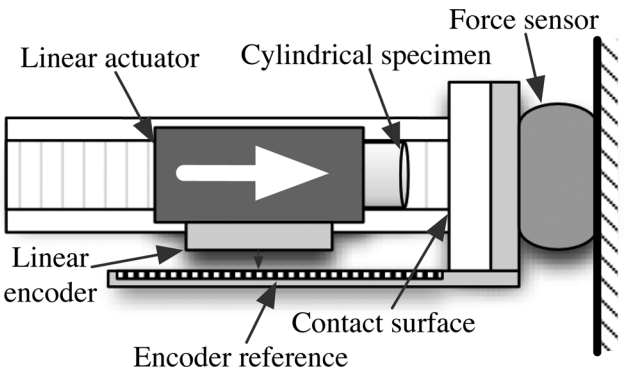

Fig. 3 Normal force configuration of the apparatus

magnesium surface was polished to 1500 grit but quickly dulled due to oxidation.

The magnesium alloy was determined to have a higher modulus of elasticity in the extruded direction than the transverse directions, meaning the material is anisotropic. Experimental results for point contact with this material may not follow Hertz law, as the theory assumes isotropy [8].

These materials are more compliant than the payload, so it is assumed that the majority of the deformation will take place in the contact surface rather than the payload. Using Young's Modulus (listed in Table 1) for each material as a rough measure of relative stiffness, it is estimated that the payload will account for approximately one-fourth of the compliance when applied to aluminum and one-sixth with magnesium AZ31. However, we can still use Eq. (11) for the normal force, since it retains the same form if both bodies are deformable [19].

Payload Geometries. Both a spherical and a flat cylindrical payload were employed.

The spherical payload has the advantage of being indifferent to alignment due to its shape. Results from the validation can also be compared with those of Hertz theory for sphere-on-plane contact.

Table 1 Material Properties for Contact Surfaces and Payload

Material	Modulus of Elasticity E (GPa)	Poisson's Ratio ν
AZ31 Magnesium	35–40	0.35
6061 Aluminum	69	0.33
316 stainless steel	200	0.27

The Hertzian contact force is given by Eq. (1). A theoretical value for Hertzian stiffness k can be determined by [8]

$$k = \frac{4}{3} E^* r^{1/2} \tag{24}$$

where r is the radius of the sphere, which in this case was 9.52 mm. E^* is defined by the elastic properties of the materials,

$$\frac{1}{E^*} = \frac{1-\nu_i^2}{E_i} + \frac{1-\nu_j^2}{E_j} \tag{25}$$

where E_i and E_j are the elastic moduli, and ν_i and ν_j are the Poisson's ratios of the bodies, found in Table 1.

For the volumetric model, the volume of interference can also be expressed in terms of depth of penetration δ [21],

$$V = \frac{\pi}{3} \delta^2 (3r - \delta) \tag{26}$$

where r is the radius of the sphere.

For the second payload, a cylinder was selected because it provided a relatively large conforming contact surface that would demonstrate the usefulness of the model in cases where point contact could not be used. Also, because contact pressure is spread over a larger surface area than with sphere-on-sphere or sphere-on-plane, there is less risk of plastic deformation from a highly concentrated point load. Finally, assuming the payload and the contact surface are perfectly aligned, the volume of interference between the cylinder and the plane can easily be expressed in terms of the depth of penetration δ,

$$V = \pi r^2 \delta \tag{27}$$

where r is the radius of the cylinder, which is 5 mm in this case. Thus, the volume of interference and, consequently, the normal force in the model have a linear relationship with the displacement. In the quasi-static case,

$$f_n = k_v \pi r^2 \delta \tag{28}$$

While Hertz point contact models cannot be used for a flat cylinder in contact with a plane, other classical solutions exist. Sneddon [22] determined the relation between force and displacement for a rigid cylindrical punch on an elastic half-space,

$$f_n = 2 r E^* \delta \tag{29}$$

where r is the radius of the cylindrical punch and E^* is defined by the elastic properties of the half space. In the case where the punch is also compliant (as it is in the case of these experiments), we can use Eq. (25) to find E^* in terms of the properties of both bodies.

When Eq. (28) and Eq. (29) are compared, we note that both models are linear in terms of δ. From these equations, a theoretical value for the volumetric stiffness can be determined,

$$k_v = \frac{2E^*}{\pi r} \tag{30}$$

Experimental results can be compared with this theoretical value. In this case, k_v is dependent on the radius of the payload. This suggests that volumetric stiffness may not be invariant with respect to geometry but may have an inverse relationship with the size of the contact patch.

3 Results and Discussion

Results for quasi-static experiments to measure volumetric stiffness with spherical and cylindrical specimens, and dynamic experiments to measure hysteretic damping with a spherical specimen are presented and discussed below.

Table 2 Hertzian and Volumetric Stiffnesses for Spherical Payload

Material	Experimental Hertzian stiffness $\left(\frac{N}{m^{1.5}}\right)$	Theoretical Hertzian stiffness $\left(\frac{N}{m^{1.5}}\right)$	Volumetric stiffness $\left(\frac{N}{m^3}\right)$
Magnesium	3.02×10^9	4.66×10^9	3.82×10^{13}
Aluminum	4.79×10^9	7.34×10^9	7.59×10^{13}

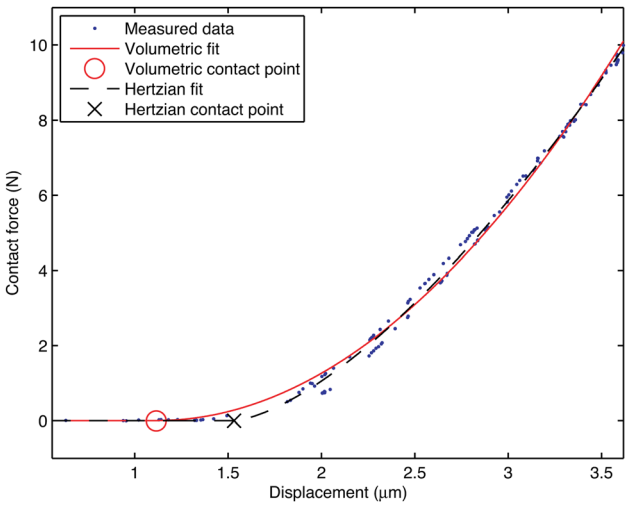

Fig. 4 Quasi-static force versus displacement for spherical contact on aluminum

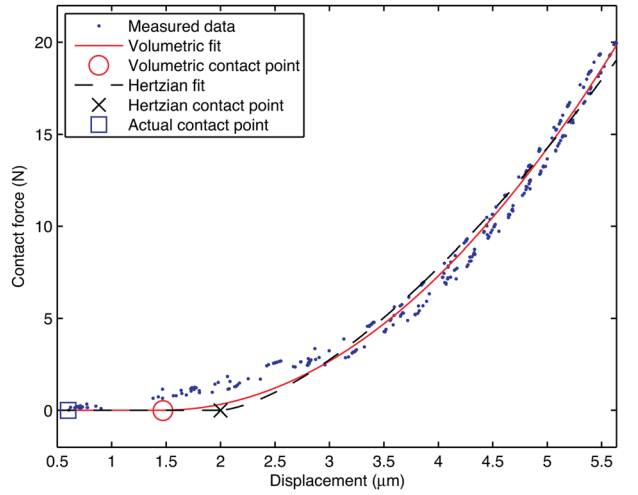

Fig. 5 Quasi-static force versus displacement for spherical contact on magnesium alloy

3.1 Volumetric Stiffness

Spherical Payload. The spherical payload was applied to each of the contact surfaces with up to 20 N of force. Using nonlinear optimization of Eqs. (19) and (20), contact points and stiffness parameters were determined for both the volumetric and Hertzian models, respectively. Stiffness values are presented in Table 2 and measured values and model fits are shown in Figs. 4 and 5. Measured Hertzian contact stiffnesses were about 2/3 of theoretical values determined using Eq. (24) for both contact surfaces. Note

that in the figures, the zero point along the horizontal axis does not correspond to the point of contact but to the relative position with respect to the initial position of the experiment. Contact points are found by fitting the model to the data.

Both models provide good fits of the measured forces and displacements. For the aluminum, the Hertzian model provides a closer fit of the data compared with the volumetric model, while for the magnesium, the volumetric model provides a closer fit. However, it should be recalled that the magnesium alloy is anisotropic, so the surface cannot be expected to behave according to Hertz law as predicted earlier.

Figures 4 and 5 show that the estimated contact point is different for the volumetric and Hertzian models. For the metals, this difference is less than half a micron, which should not significantly impact the simulation of larger robotic tasks. The expressions for force have different orders with respect to displacement around the point of contact for the models. Using "Big O" notation for the Hertzian model and volumetric models,

$$F_{\text{Hertz}} = O(\delta^{1.5}) \quad \text{as} \quad \delta \to 0 \tag{31a}$$

$$F_{\text{vol}} = O(\delta^{2}) \quad \text{as} \quad \delta \to 0 \tag{31b}$$

Thus, near the contact point, the estimated force will rise more rapidly for the Hertzian model than for the volumetric model. Since the force-displacement slope for the volumetric profile is numerically shallower, the nonlinear optimization will tend to estimate the contact point occurring for the volumetric model slightly ahead of the Hertzian model.

The "actual" measured point of contact (based on where contact forces are first detected) differs from points of contact estimated from nonlinear optimization with the magnesium sample (Fig. 5). There is an initial region of lower slope for the first few microns in the force-displacement curve that is not accounted for in either model.

The initial contact region for magnesium may be accounted for by the asperities of the contact surface. The surface of the magnesium sample was smoothed to a reflective 1500 grit, or 3 μm, but rapidly became dull. These surface asperities reduce the surface area of the contact patch, leading to a much lower force-displacement slope until these asperities have been flattened. In addition, the elastic properties of the oxidized magnesium surface is unknown and may account for this initial difference.

A small amount of hysteresis is observed in the measurements for both materials, such that there is slightly less contact force when the payload is being reversed as compared to when it is applied. Since the payload is allowed to rest after reaching each servo encoder count, this hysteresis cannot be attributed to velocity-dependent damping forces in the model. The amount of hysteresis will increase with higher maximum loads, suggesting some small amount of permanent deformation is taking place. The volumetric model does not account for velocity dependent plastic deformation. For contact scenarios where deformation is more pronounced, other approaches, such as the deformation model by Vu Quoc et al. [14,15], may be required. In this case, the hysteresis is not significant.

Cylindrical Payload. Measurements using a cylindrical payload are shown in Figs. 6 and 7. Attempts at a linear fit of the data are shown as a solid line, labeled "Perpendicular fit." The results do not conform well to a linear fit, which the volumetric model would call for. Classical elastic theory would also suggest a linear fit between displacement and force for a perpendicular cylinder on a plane. This suggests that there are non-negligible surface asperities on the cylindrical payload or that the surfaces are misaligned. Additionally, estimated stiffness values (Table 3) are two orders of magnitude less than theoretically predicted in Eq. (30).

Sources of misalignment in the experiment may include the mounting of the payload to the ball screw (along the horizontal axis in the plane of the contact surface) and the relative alignments of the ball screw and the force sensor (along the vertical axis).

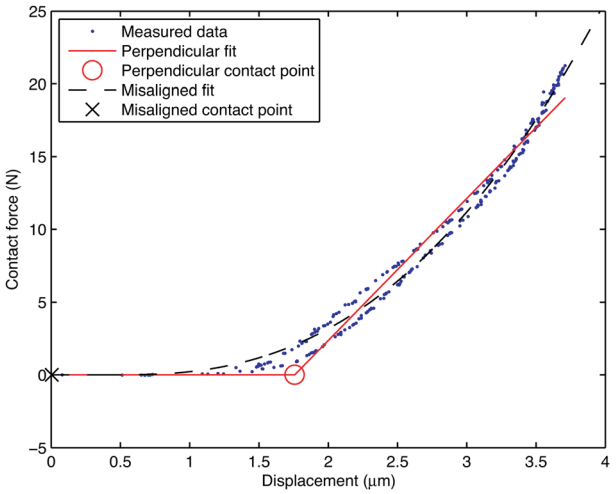

Fig. 6 Quasi-static force versus displacement for cylindrical contact on aluminum

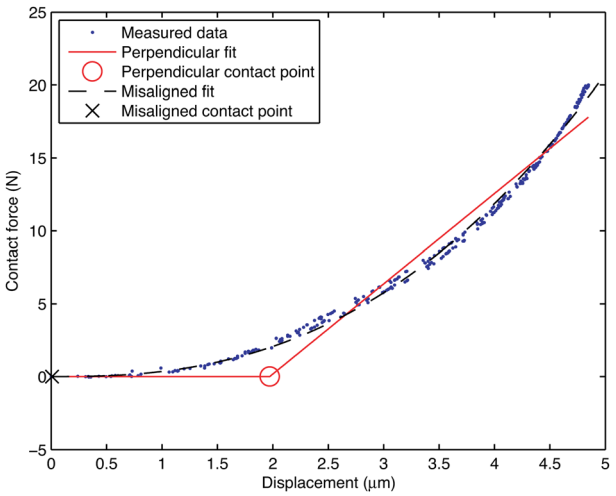

Fig. 7 Quasi-static force versus displacement for cylindrical contact on magnesium alloy

Table 3 Volumetric Stiffnesses for the Cylindrical Payload

Material	Experimental $\left(\frac{N}{m^3}\right)$	Theoretical $\left(\frac{N}{m^3}\right)$
Magnesium	7.88×10^{10}	5.17×10^{12}
Aluminum	1.24×10^{11}	8.82×10^{12}

For the purpose of modeling the contact in the misaligned case, it is assumed that angle from the normal γ does not change significantly over the loading and unloading sequence. Unfortunately, no analytical solution exists in classical contact theory for the relationship between force and displacement for an inclined cylinder on a plane with incomplete contact [23]. For the volumetric model, the volume of a cylindrical wedge [21] can be used to estimate volume of interference,

$$V = \frac{\delta r^3}{3b}\left[2\sin\phi - \cos\phi\left(3\phi - \frac{1}{2}\sin 2\phi\right)\right] \tag{32}$$

where b and ϕ are

$$b = \frac{\delta}{\tan\gamma} \quad \text{and} \quad \phi = \cos^{-1}\left(\frac{r-b}{r}\right) \tag{33}$$

In terms of parameter identification from the experimental results, this volume model yields an additional angle misalignment term γ in addition to the volumetric stiffness and contact boundary unknowns for the perpendicular case.

The stiffness parameter can be treated as known by substituting those determined from Eq. (30) and shown in Table 3. Nonlinear optimization was used to find the unknowns, and the resulting displacement-force curves for the aluminum and magnesium surfaces are shown as dashed lines in Figs. 6 and 7. The estimated off-normal angles were determined to be 0.46 deg and 0.32 deg for the magnesium and aluminum, respectively. In both cases, the misalignment is less than half a degree.

Misalignments of this small a magnitude would be very difficult to perceive visually. However, it is also possible that the payload has non-negligible surface asperities. Concentrated loads from either misalignment or non-negligible surface asperities, leading to plastic deformation, could also explain the small amount of hysteresis observed in Figs. 6 and 7. As with the spherical specimen, this hysteresis is not significant enough to require inclusion in the contact model.

3.2 Damping. As spherical payloads offered results in quasi-static testing that agreed well with the model, spherical payloads were employed for the dynamic tests. The hard metallic contact surfaces were impacted at speeds ranging from 0.1 to 1 mm/s. The motor controller was programmed to track the desired velocity using the signal from the internal encoder of the servo. The servo encoder, when connected to the ball screw system, had a resolution of 1.25 μm per encoder count. With a frequency of 16 kHz, the LabVIEW controller was observed to maintain the desired velocity to within about 0.1 mm/s due to the small number of servo encoder counts between time intervals.

Measurements of force and position commenced prior to contact with a sampling frequency of 1 kHz. Accurate measurements of the position of the payload came from the high resolution linear encoder. Once contact had occurred, the motor would continue to attempt to track the desired velocity. Due to the compliance in the ball screw system and the apparatus, the actual velocity of the payload itself relative to the contact surface slowed down even though the speed of the motor was maintained.

At least one second of force and displacement measurements were collected during a collision. A subset of the sampled data was then selected for comparison with the model with the following methodology. For each collision, the position contact where contact first occurred was estimated from the force data. The preprocessor then selects 0.1 s of data, beginning at a point two servo encoder counts (2.5 μm) prior to contact. An example of such a sample is shown in Fig. 8.

With the position data, the volume of interference can be determined allowing the contact force without damping effects to be estimated for each sampled position. Experimental volumetric stiffness values determined with the spherical payload are used. These estimated force values in the case of Fig. 8 are shown as a dashed line in the lower force graph. It is observed that these estimates are lower than the sampled force values, indicating that damping has occurred.

The final force modeled using position data, with an estimated damping factor of 1.6×10^4s/m, is shown in Fig. 8 as a solid line. The line appears noisy due to the speed estimates. At very low speeds, there is only a small number of encoder counts between sample intervals. The effect of the error in speed estimates on the magnitude of the estimated force is increased as the penetration depth increases.

Measured Damping Factors. Measured values of the hysteretic damping factor for the magnesium alloy and aluminum are shown

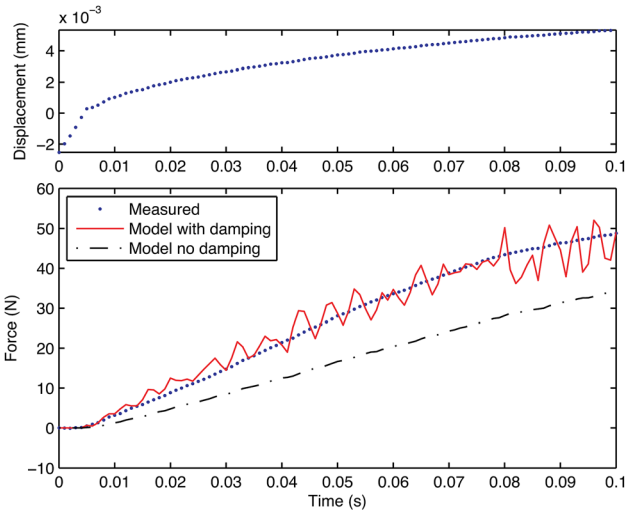

Fig. 8 Force and displacement measurements for impact at 0.58 mm/s on magnesium alloy

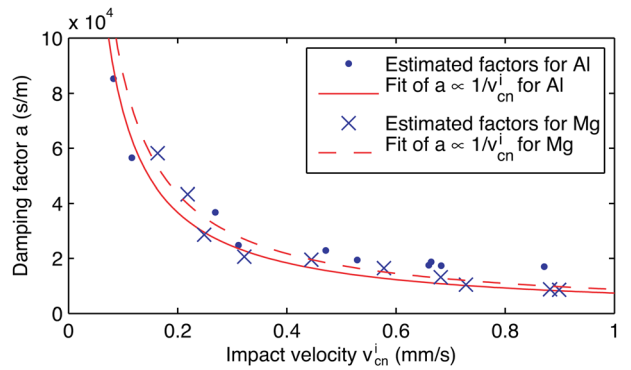

Fig. 9 Estimated hysteretic damping factors plotted by impact velocity

in Fig. 9. It is observed that the damping factor can be inversely related to the initial impact velocity. A least-squares fit of an inverse relation is shown in the figures as solid and dashed lines for aluminum and magnesium, respectively.

As the payload is driven by the motor into the contact surface and is not in "free collision," the concept of a coefficient of restitution does not apply. However, the inverse relationship between the hysteretic damping factor a and the impact velocity observed is similar to Eq. (12), as long as the coefficient of restitution e is assumed to be constant with respect to v^i_{cn}. This coefficient e was found to be 0.134 for aluminum and 0.114 for magnesium.

3.3 Sources of Error. As discussed in the cylindrical payload results, it is possible that the apparatus is not well aligned. In the spherical payload case, this minor misalignment should have negligible impact on results. However, in the case of the cylindrical payload, even small misalignments may result in incomplete contact over the course of the experiment.

Surface asperities are also a plausible cause for the nonlinearity of the cylindrical measurements, since the surfaces have not been smoothed to a mirror finish. Surface roughness has been found to be a significant factor in the reduction of contact stiffness, both theoretically and experimentally [24]. Polished, the payloads and contact surfaces should have surface asperities no greater than a few microns. Note that the magnesium dulled quickly after polishing (as expected). It is not known what impact this oxidation had on the properties of the magnesium.

The range of contact loads presented was limited by the experimental apparatus. At higher loads, there is compliance in the plate holding the encoder reference to the force sensor. Forces in the quasi-static experiments were limited to 20 N so that deflection of the position equipment was negligible. This limitation is a consequence of the design of the apparatus and should be addressed for future experiments.

The motor driving the linear actuator was a source of vibration to the payload. Since damping is the result of vibrations dissipating away energy, the vibration of the motor may have had some impact on the accuracy of the dynamic experiments. Further investigation, including performing dynamic experiments with the payload decoupled from the motor, is required.

4 Conclusions

A volumetric contact dynamics model based on the Winkler elastic foundation model is presented for validation. Forces are expressed in terms of the properties of the volume of interference between the solid geometries of the bodies in contact.

A series of experiments and an apparatus have been presented to validate the model of the normal contact force in static and dynamic conditions and to identify volumetric stiffness and hysteretic damping factors. Experiments were performed using a spherical payload on a planar surface in order to compare with more commonly used Hertzian models and a cylindrical payload on a planar surface in order to provide a relatively large contact surface area and so that the relationship between volume of interference and measured displacement should be linear according to the model. Contact surfaces of magnesium alloy and aluminum were used against stainless steel payloads.

Quasi-static experiments were used to determine and validate Hertzian and volumetric stiffness. For spherical payload experiments, Hertzian stiffnesses were about $2/3$ of theoretical values, suggesting the measurements performed with the apparatus were reasonable. Volumetric stiffnesses were determined to be $3.82 \times 10^{13}\mathrm{N/m^3}$ and $7.59 \times 10^{13}\mathrm{N/m^3}$ for magnesium and aluminum, respectively. For the cylindrical payload, assuming perpendicular contact resulted in volumetric stiffness estimates several orders of magnitude lower. Using stiffnesses determined from spherical experiments, small misalignments in the apparatus were estimated that corresponded well with measured results.

Damping experiments were also performed with the spherical payload to measure velocity-dependent hysteretic damping. As anticipated, contact forces increased with greater impact speed. The hysteretic damping for the volumetric model was determined to be inversely related to impact speed. For this constrained motion where the payload is driven by the linear motor, the coefficient of restitution then remains constant.

Future efforts include improving the acceptable force range of the experimental apparatus, better alignment of the payload, and extending the apparatus for friction experiments.

Acknowledgment

We would like to acknowledge the support of Dr. Yves Gonthier of the Canadian Space Agency (CSA).

Funding for this research was provided by the Natural Sciences and Engineering Research Council of Canada (NSERC) and the CSA.

References

[1] de Carufel, J., Martin, E., and Piedbœuf, J.-C., 2000, "Control Strategies for Hardware-In-The-Loop Simulation of Flexible Space Robots," IEEE Proc.: Control Theory Appl., **147**(6), pp. 569–579.
[2] Gonthier, Y., McPhee, J., Lange, C., and Piedbœuf, J.-C., 2004, "A Regularized Contact Model With Asymmetric Damping and Dwell-Time Dependent Friction," Multibody Syst. Dyn., **11**(3), pp. 209–233.
[3] Gilardi, G., and Sharf, I., 2002, "Literature Survey of Contact Dynamics Modelling," Mech. Mach. Theory, **37**, pp. 1213–1239.
[4] Hertz, H., 1896, *Miscellaneous Papers by H. Hertz*, D. E. Jones and G. Schott, eds., Macmillan, London.
[5] Hunt, K., and Crossley, F., 1975, "Coefficient of Restitution Interpreted as Damping in Vibroimpact," J. Appl. Mech., **7**, pp. 440–445.
[6] Janabi-Sharifi, F., 1995, "Collision: Modeling, Simulation and Identification Of Robotic Manipulators Interacting With Environments," J. Intell. Robotic Syst., **13**(1), pp. 1–44.
[7] Lankarani, H. M., and Nikravesh, P. E., 1994, "Continuous Contact Force Models for Impact Analysis in Multibody Systems," Nonlinear Dyn., **5**, pp. 193–207.
[8] Johnson, K., 1985, *Contact Mechanics*, Cambridge University Press, London.
[9] Goldsmith, W., 1960, *Impact: The Theory and Physical Behavior of Colliding Solids*, Edward Arnold Ltd., London.
[10] Marhefka, D., and Orin, D., 1999, "A Compliant Contact Model With Nonlinear Damping for Simulation of Robotic Systems," IEEE Trans. Syst., Man Cybern., Part A. Syst. Humans, **29**(6), pp. 566–572.
[11] Flores, P., Machado, M., Silva, M., and Martins, J., 2011, "On the Continuous Contact Force Models for Soft Materials in Multibody Dynamics," Multibody Syst. Dyn., **25**, pp. 357–375.
[12] Diolaiti, N., Melchiorri, C., and Stramigioli, S., 2005, "Contact Impedance Estimation for Robotic Systems," IEEE Trans. Rob., **21**(5), pp. 925–935.
[13] Stoianovici, D., and Hurmuzlu, Y., 1996, "A Critical Study of the Applicability of Rigid-Body Collision Theory," ASME J. Applied Mech., **63**, pp. 307–316.
[14] Vu-Quoc, L., and Zhang, X., 1999, "An Elasto-Plastic Contact Force-Displacement Model in the Normal Direction: Displacement-Driven Version," Proc. R. Soc. London, Ser. A, **455**(1991), pp. 4013–4044.
[15] Vu-Quoc, L., Zhang, X., and Lesburg, L., 2000, "A Normal Force-Displacement Model for Contacting Spheres, Accounting for Plastic Deformation: Force-Driven Formulation," J. Appl. Mech., **67**(2), pp. 363–371.
[16] Zhang, X., and Vu-Quoc, L., 2002, "A Method to Extract the Mechanical Properties of Particles in Collision Based on a new Elastoplastic Normal Force-Displacement Model," Mech. Mater., **34**(12), pp. 779–794.
[17] Plantard, G., and Papini, M., 2005, "Mechanical and Electrical Behaviors of Polymer Particles. Experimental Study of the Contact Area Between two Particles. Experimental Validation of a Numerical Model," Granular Matter, **7**(1), pp. 1–12.
[18] Gonthier, Y., McPhee, J., Lange, C., and Piedbœuf, J.-C., 2005, "A Contact Modeling Method Based on Volumetric Properties," Proceedings of the 2005 ASME Design Engineering Technical Conferences and 5th International Conference on Multibody Systems, Nonlinear Dynamics and Control, Vol. 2005, pp. 477–486.
[19] Gonthier, Y., 2007, "Contact Dynamics Modelling for Robotic Task Simulation," Ph.D. thesis, University of Waterloo, West Waterloo, ON, Canada.
[20] Roy, A. R., and Carretero, J. A., 2009, "A volume-Based Contact Dynamics Model With Asymmetric Damping Independent of the Coefficient of Restitution," Proceedings of the 2009 CCToMM Mechanisms, Machines, and Mechatronics Symposium.
[21] Harris, J. W., and Stocker, H., 1998, *Handbook of Mathematics and Computational Science*, Springer-Verlag, New York.
[22] Sneddon, I. N., 1965, "The Relation Between Load and Penetration in the Axisymmetric Boussinesq Problem for a Punch of Arbitrary Profile," Int. J. Eng. Sci., **3**(1), pp. 47–57.
[23] Munisamy, R. L., Hills, D. A., and Nowell, D., 1995, "The Solution of the Contact Between a Tilted Circular Rigid Punch and an Elastic Half-Space," Wear, **184**(1), pp. 93–95.
[24] Verscheure, D., Sharf, I., Bruyninckx, H., Swevers, J., and Schutter, J. D., 2009, "Identification of Contact Dynamics Parameters for Stiff Robotic Payloads," IEEE Trans. Rob., **25**(2), pp. 240–252.